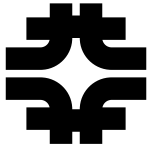

Fermi National Accelerator Laboratory

FERMILAB-Pub-97/239

Measurement of Proton-Induced Radiation Damage Effects in Double-Sided Silicon Microstrip Detectors

A. Brandl, S. Seidel and S. Worm
For the CDF Collaboration

The New Mexico Center for Particle Physics
The University of New Mexico
Albuquerque, New Mexico 87131

Fermi National Accelerator Laboratory
P.O. Box 500, Batavia, Illinois 60510

July 1997

Submitted to *Nuclear Instruments and Methods*

Operated by Universities Research Association Inc. under Contract No. DE-AC02-76CH03000 with the United States Department of Energy

Disclaimer

This report was prepared as an account of work sponsored by an agency of the United States Government. Neither the United States Government nor any agency thereof, nor any of their employees, makes any warranty, expressed or implied, or assumes any legal liability or responsibility for the accuracy, completeness, or usefulness of any information, apparatus, product, or process disclosed, or represents that its use would not infringe privately owned rights. Reference herein to any specific commercial product, process, or service by trade name, trademark, manufacturer, or otherwise, does not necessarily constitute or imply its endorsement, recommendation, or favoring by the United States Government or any agency thereof. The views and opinions of authors expressed herein do not necessarily state or reflect those of the United States Government or any agency thereof.

Distribution

Approved for public release; further dissemination unlimited.

Measurement of Proton-Induced Radiation Damage Effects in Double-Sided Silicon Microstrip Detectors

A. Brandl, S. Seidel, S. Worm

The New Mexico Center for Particle Physics
The University of New Mexico
Albuquerque, NM, 87131 USA

15 April 1997

Abstract

The electrical characteristics of double-sided n-type silicon microstrip detectors were investigated after those detectors had received proton irradiation up to a fluence equivalent to 1.7×10^{13} 1 MeV neutrons/cm^2. This fluence is about twice as much as is expected for the CDF SVX II innermost layer during its first year. It is also approximately equal to the fluence expected at a radius of 12 cm from an interaction point during the first three years of operation of an LHC experiment. The detectors' p- and n-side leakage currents and their depletion voltages responded to the damage in a manner consistent with present models. Their total capacitance per active length increased by $(2.0 \pm 0.7) \times 10^{-14}$ pF-cm/[1 MeV neutron] on the p-side. Their total capacitance increased by $(1.5 \pm 0.1) \times 10^{-13}$ pF-cm^2/[1 MeV neutron] on the n-side for a particular double-metal geometry. Their coupling capacitance was unchanged by this fluence. The study required development of a new method for determining full depletion voltage; that method is also presented here.

1 Introduction

Eight double-sided silicon microstrip detectors which were manufactured with n-type substrates by SINTEF/SI have been electrically characterised. The detectors, which are prototypes for the SVX II [1], received irradiation by 500 MeV protons at TRIUMF. The fluence was normalized to its 1 MeV neutron equivalent, denoted here as $\langle n \rangle/cm^2$. The maximum fluence received by the detectors is about twice the fluence expected to be received by the inner layer of the SVX II during the first year [2]. It is also similar to what would be received by a sensor at a radius of 12 cm from an interaction point during the first three years of operation of an LHC experiment [3]. Since dose-dependent modification of some of the detectors' electrical properties was expected, their p- and n-side leakage currents, depletion voltages, and coupling and total capacitances were investigated.

We regard the total capacitance measurement to be the principal contribution of this paper; current and voltage measurements are also presented to demonstrate that the irradiated sensors behaved according to established models. The n-side current measurements are also reported here to demonstrate a new technique for determining full depletion voltage.

In Table 1, some distinguishing features of the detector types are summarized. All detectors have double-metal readout on the n-side. The insulator used in the double-metal structure is polyimide. Bias voltage is applied through polysilicon resistors. The implants on the p- and n-sides are 9 μm and 11 μm wide, respectively; and the detectors are 280 μm thick. Additional information can be found in Reference [4].

Table 1: Features of the Detectors

Type	Intermediate Strips	Nominal Length (cm)	Nominal Width (cm)	p-side Implant Pitch (μm)	n-side Implant Pitch (μm)
A	p-side	4.25	2.07	25	103
B	none	4.25	2.07	50	103
D	none	8.50	1.43	50	158

Table 2 summarizes the radiation levels received by the detectors. Radia-

tion exposures were done in 1994 and 1995; the fluence during each exposure is listed separately.

Table 2: Fluence Received by the Detectors

Detector Name	Type	Fluence		
		1994 ($\langle n\rangle/cm^2$)	1995 ($\langle n\rangle/cm^2$)	Total ($\langle n\rangle/cm^2$)
db19	A	0	0	0
db21	B	0	0	0
db8	D	0	0	0
db6	D	$(4.7\pm1.3)\times10^{12}$	0	$(4.7\pm1.3)\times10^{12}$
db12	B	$(2.4\pm0.2)\times10^{12}$	$(2.7\pm0.5)\times10^{12}$	$(5.1\pm0.5)\times10^{12}$
db29	B	0	$(1.4\pm0.2)\times10^{13}$	$(1.4\pm0.2)\times10^{13}$
db27	A	$(2.4\pm0.2)\times10^{12}$	$(1.3\pm0.2)\times10^{13}$	$(1.5\pm0.2)\times10^{13}$
db30	B	$(2.5\pm0.3)\times10^{12}$	$(1.4\pm0.2)\times10^{13}$	$(1.7\pm0.2)\times10^{13}$

The detectors in this batch were all mounted in printed circuit boards which held the preamplifiers. On each detector side, 128 strips were wire-bonded to an SVX2 chip [5]. The bias traces and the guard ring were connected through wire bonds to a noise filter circuit and then to connectors through which the bias voltage could be applied.

Characterisation of the detectors was done by selecting a sample of 5 to 9 readout strips per side. The sample strips were evenly distributed across the entire detector width or length. The strips that were wire-bonded to the SVX2 chip could not be probed directly and were consequently excluded from the sample. Detector properties were then estimated through interpolation of the samples.

Most of the techniques used to make the electrical measurements are explained in References [6] and [7]. Some additional techniques were developed to accommodate the facts that the detectors were mounted to boards and that low-pass filters on the boards introduced additional capacitances; those techniques are explained in the sections that follow.

2 Measurements

2.1 p-side Leakage Current

Radiation damage in the bulk of a silicon microstrip detector is expected to increase the leakage current density, $J_{\mathrm{irradiated}}$, in direct proportion to the fluence, Φ, of damaging particles:

$$J_{\mathrm{irradiated}} = \alpha\Phi + J_{\mathrm{intrinsic}} \tag{1}$$

where α is an empirical damage constant (the fluences were normalized to $\langle \mathrm{n} \rangle/\mathrm{cm}^2$, so the damage constant for neutrons was used: $\alpha = (2.86 \pm 0.18) \times 10^{-17}$ A/cm [8]), and $J_{\mathrm{intrinsic}}$ is the intrinsic leakage current density which is a property of the undamaged bulk silicon.

The active area leakage current could not be measured directly, since the detectors' guard rings and bias traces were connected through wire bonds. The leakage currents per strip were measured, averaged, and then multiplied by the total number of strips to obtain an estimate of the active area leakage current. For the measurement of the leakage current per individual p-side strip, a positive bias potential was applied to the backplane, the n-side, of the detector. The p-side guard ring and bias trace were grounded through a probe. The individual p-side implant was then connected to the ammeter by touching a probe to its contact pad.

Table 3 summarizes the post-irradiation average leakage current per strip, the (interpolated) leakage current for the total active area, and the pre- and post-irradiation leakage current per unit active detector area [9] for the five detectors.

The leakage currents given in Table 3 were calculated by extrapolation [10] of the measured values to 25°C. The operating voltage used was the measured depletion voltage (see Sect. 2.3) plus 10 V. The variation between individual strips is reflected by the standard deviations about the mean values. The post-irradiation p-side leakage currents of db6 and db12 were unable to be measured.

Systematic errors due to variation of the ambient temperature during measurement, Joule heating caused by current flow in the bulk, and contact

Table 3: p-side Leakage Current in the Detectors

Detector Name	Leakage Current			
	Post-Irradiation			Pre-Irradiation
	per Strip (μA)	Total (μA)	per Unit Active Area (μA/cm^2)	per Unit Active Area (μA/cm^2)
db6	—$^\diamond$	—	—	0.3±0.1
db12	—$^\diamond$	—	—	$(1.4\pm0.2)\times10^{-3}$
db29	$(2.9\pm0.1)\times10^{-1}$	110±4.5	15±1.0	0.3±0.1
db27	$(1.7\pm0.1)\times10^{-1}$	130±6.2	13±0.6	0.3±0.1
db30	$(3.3\pm0.2)\times10^{-1}$	130±8.5	16±0.8	$(7.7\pm0.8)\times 10^{-2}$

$^\diamond$ No p-side single strip leakage current measurement possible.

potentials associated with the placement of the probes were investigated and found not to exceed 9 nA/cm^2 for both unirradiated and irradiated detectors. The systematic error due to mounting the detectors was estimated by comparing the leakage current in the three unirradiated detectors before and after mounting. This systematic error was found to be less than 0.1 μA/cm^2. The errors quoted in Tables 3, 4, and 5 reflect the quadrature sum of statistical and systematic uncertainties.

2.2 n-side Leakage Current

The measurement of the total n-side leakage current was expected to give results consistent with the value of the total p-side leakage current. In order to verify this prediction, 12 to 15 evenly distributed n-side strips were investigated per detector.

The experimental setup for the measurement of the n-side leakage current was similar to that for the p-side leakage current. A negative voltage was applied through the p-side bias ring. The n-side bias trace was grounded through a probe; the probe connected to the electrometer was placed on the DC pad under test.

The leakage currents of individual n-side strips were found to be highly position-dependent. Comparison of the leakage currents with damage profiles taken from calibration foils confirmed this to be due to their spatially

non-uniform irradiation.

Typical single-strip leakage currents for the n-sides of detectors that received different levels of irradiation are depicted in Figure 1. It is apparent that the shape of a plot of the leakage current of a single n-side strip versus the applied bias voltage changes dramatically with radiation damage. In an uninverted detector, prior to full depletion, n-side strips are not isolated, so the leakage current detected from a single strip is drawn from a large volume of the bulk. When $V_{\text{depletion}}$ is reached, the leakage current drops sharply to that of a single strip. (Typically the transition occurs over a range of 10 to 20 Volts.) The location of the transition in Figure 1 changes significantly with irradiation. The single strip current is given by the lowest current found above full depletion. As with the p-side leakage current measurements, the systematic error on the n-side is less than 3%.

The total n-side leakage current was estimated by integrating the area underneath the curves that were generated by interpolating between data points from the individual strips. Table 4 shows the total n-side leakage currents and the leakage currents per unit active detector area.

Table 4: n-side Leakage Current in the Detectors

Detector Name	Post-irradiation n-side Leakage Current	
	Total (μA)	per Unit Active Area (μA/cm^2)
db6	55±6.6	5.2±0.6
db12	24±2.9	2.9±0.4
db29	150±15	18±1.8
db27	110±4.0	13±0.5
db30	130±13	16±1.6

Table 5 compares the measured p- and n-side leakage currents of all of the detectors. All measured leakage currents were found to be consistent with the model in Reference [8].

The general consistency of the p- and n-side currents suggests that it is appropriate to use their average value for comparisons with theoretical predictions. Table 5 compares this average measured leakage current with

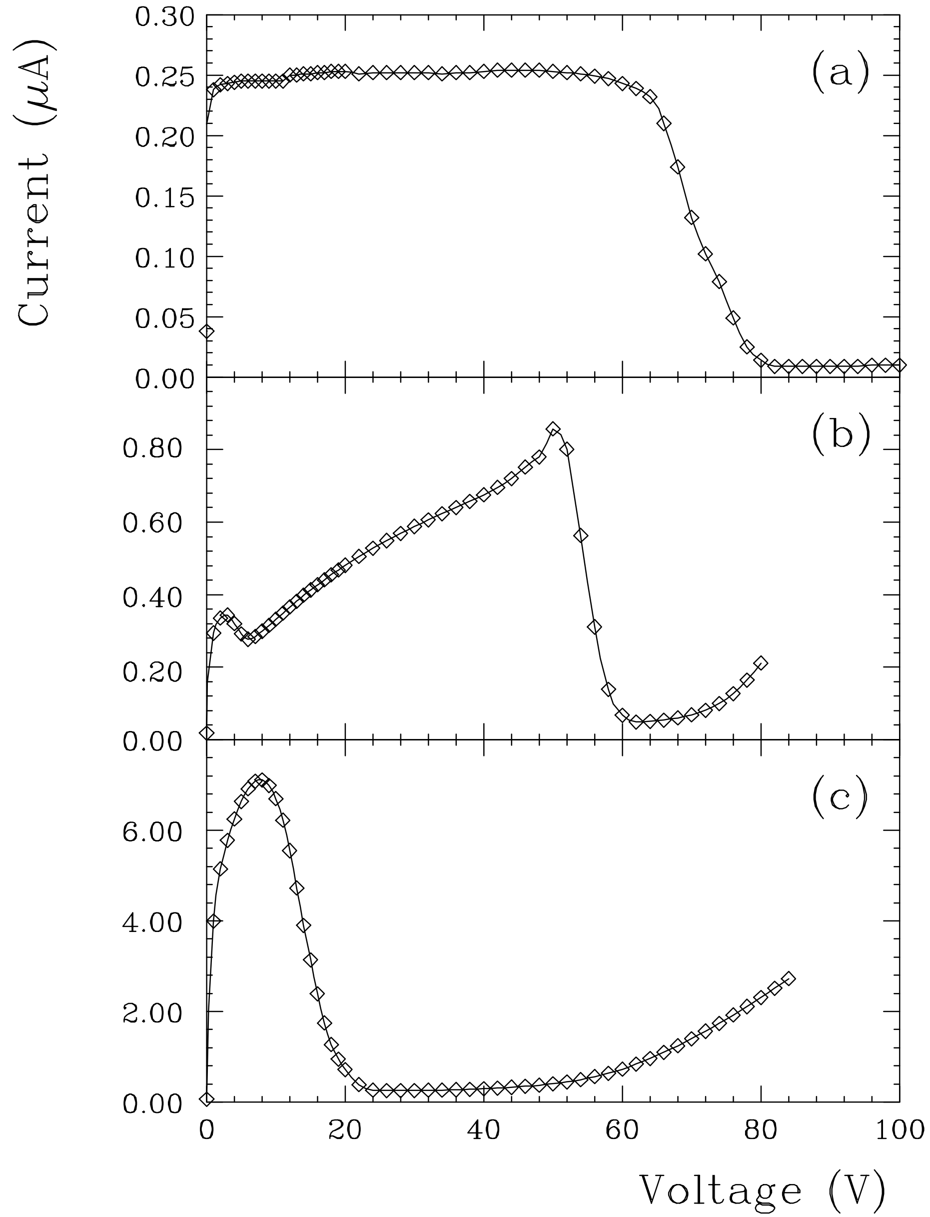

Figure 1: n-side current versus voltage for detectors with different amounts of radiation damage: (a) db19 with 0 $\langle n \rangle/cm^2$, (b) db12 with 5.1×10^{12} $\langle n \rangle/cm^2$, and (c) db29 with 1.4×10^{13} $\langle n \rangle/cm^2$.

that predicted by Equation 1. The measured p-side pre-irradiation currents are used as input for both the p- and n-side calculations; they are taken from Reference [9]. The measured and predicted post-irradiation values are found to be consistent for all detectors.

Figure 2 shows the average of the measured p- and n-side leakage currents per unit active area as a function of the fluence of damaging particles.

Table 5: Comparison between Expected and Measured Leakage Current per Unit Active Area for the Detectors

Detector Name	Leakage Current per Unit Active Area			α Estimated from Averaged p- and n-side Leakage Current
	Expected	Measured		
		p-side	n-side	
	(μA/cm^2)	(μA/cm^2)	(μA/cm^2)	($\times 10^{-17}$ A/cm)
db19	0.3±0.1	0.3±0.1	0.3±0.1	—*
db21	0.3±0.1	0.4±0.1	0.4±0.1	—*
db8	0.3±0.1	0.4±0.1	0.7±0.2	—*
db6	4.1±1.1	—†	5.2±0.6	3.7±1.3‡
db12	4.1±0.5	—†	2.9±0.4	2.0±0.4‡
db29	12±1.8	15±1.0	18±1.8	4.0±0.8
db27	12±1.8	13±0.6	13±0.5	3.0±0.4
db30	14±1.8	16±0.8	16±1.6	3.3±0.5

* Unirradiated detectors.
† A post-irradiation p-side current measurement is not available for these detectors.
‡ For these detectors, α is estimated from the n-side current only.

2.3 Depletion Voltage

The depletion voltage is expected to change according to

$$V_{\text{depletion}} = \frac{|N_{\text{eff}}| q d^2}{2\epsilon_{\text{Si}}} \tag{2}$$

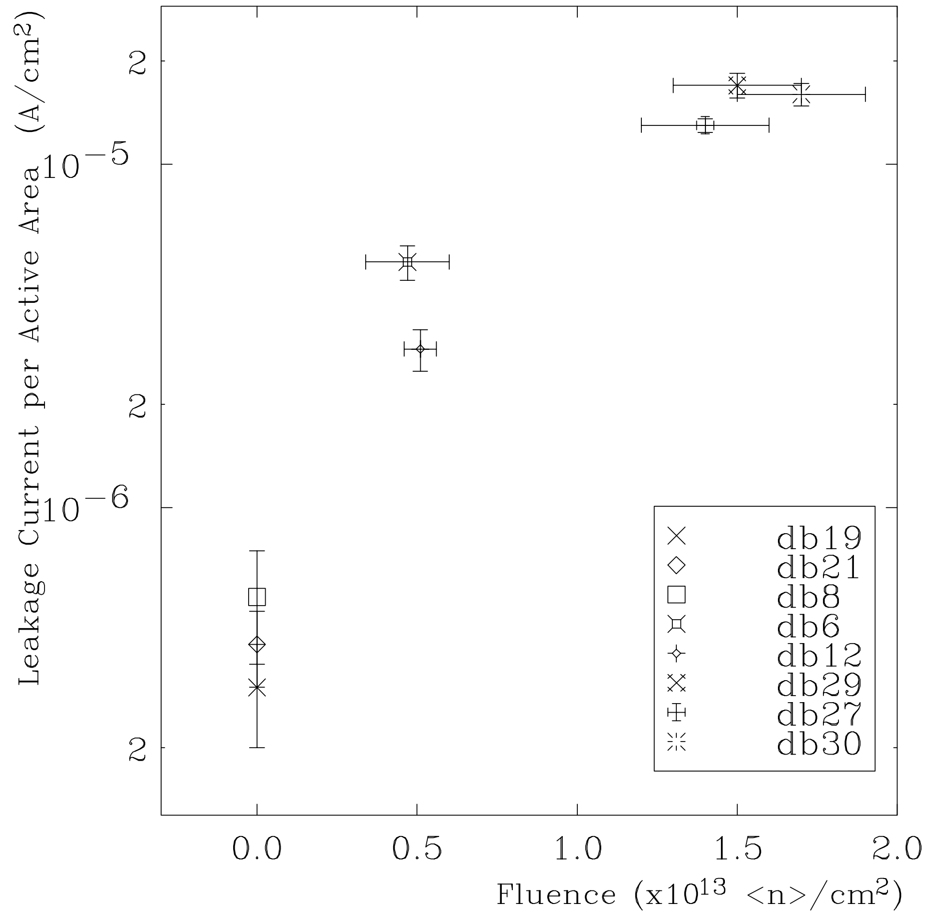

Figure 2: Average of the p- and n-side leakage currents per active area, as a function of 1 MeV neutron equivalent fluence, for the detectors. (For detectors db6 and db12, for which no p-side current measurement is available, the average is replaced by the n-side current alone.)

where q is the electron charge, d is the detector thickness, and ϵ_{Si} is the permittivity of silicon. N_{eff} is given by [8]

$$N_{\mathrm{eff}}(\Phi) = N_{\mathrm{eff},0} - N_{C0}(1 - e^{-c\Phi}) - g_C\Phi - g_Y\Phi\left(1 - \frac{1}{1 + g_Y\Phi k(T)t}\right) \quad (3)$$

where Φ is the 1 MeV neutron fluence, t is the time after irradiation, and $N_{\mathrm{eff},0}$ is the initial doping density. $N_{\mathrm{eff},0}$ was extracted from $V_{\mathrm{depletion}}$ measurements of unirradiated detectors by using Equation 2. N_{C0} is taken to be $50 \pm 15\%$ of $N_{\mathrm{eff},0}$, according to measurements reported [11] for different but comparable wafers. Values for $N_{\mathrm{eff},0}$ and for the other parameters are given in Table 6. The temperature dependence of k is given by

$$k(T) = k_{293.15}\exp\left(\frac{E_a}{k_B}\left[\frac{1}{293.15} - \frac{1}{T}\right]\right) \quad (4)$$

with values for E_a and $k_{293.15}$ also given in Table 6; k_B is the Boltzmann constant and T is temperature.

Table 6: a) $N_{\mathrm{eff},0}$ for the detectors, and b) parameters needed for the calculation of $V_{\mathrm{depletion}}$. Parameters are taken from Reference [12] and are appropriate for protons.

Detector Name	$N_{\mathrm{eff},0}$ (10^{12} cm^{-3})
db6	1.1±0.1
db12	1.0±0.1
db29	1.1±0.1
db27	1.0±0.1
db30	1.1±0.1

Parameter	Value
g_Y (10^{-2} cm^{-1})	5.8±0.3
g_C (10^{-2} cm^{-1})	1.15±0.09
c (10^{-13} cm^2)	0.96±0.19
E_a (eV)	1.31±0.04
$k_{293.15}$ (10^{-20} cm^3/s)	1.55±0.21

Table 7 shows the expected depletion voltages, as calculated from the above equations, for the irradiated detectors. The errors in the calculation

reflect the uncertainties in the received fluence and in the given constants. The depletion voltage predictions include the effects of segmentation as described in Reference [13].

Table 7: Depletion Voltage of the Detectors Predicted with Equations 2, 3, and 4.

Detector Name	Predicted Depletion Voltage (V)
db6	54±10
db12	50±9
db29	25±14
db27	13±13
db30	20±14

The results shown in Figure 1 of the n-side leakage current studies indicate that it is possible to find $V_{\mathrm{depletion}}$ for a detector by studying the leakage current, I_{leakage}, for single n-side strips as a function of the bias voltage. We believe that the voltage determined in this way represents the one at which the full volume of the detector is depleted, including the volume near the surface, between implants. Obtaining this truly full depletion is necessary for detectors used to track charged particles since otherwise, charge lost in slow-drift, partially depleted volumes can contribute to tracking inefficiency. We compare this technique for finding full depletion with two others that are commonly used. The second method uses the shape of the bulk capacitance versus applied voltage ("C-V") curve, while the third method uses pulse height versus bias voltage. Table 8 compares values of depletion voltage obtained by the three methods. The errors quoted are the quadrature sum of statistical and systematic uncertainties. The systematic uncertainties are consistent with those we have reported in Reference [14].

According to the second method, the point of inflection of the C-V curve indicates $V_{\mathrm{depletion}}$. We removed noise-filter circuits from the boards in which the detectors were mounted and then followed the procedure for this method described in Reference [7]. The low and high potential terminals of the bias isolation network were connected to the p-side and n-side guard rings and bias traces, respectively. The bias voltage from the Keithley 237 Source Measure Unit was also connected to the bias isolation network.

For the third method, pulse heights of signals stimulated in the detectors by a penetrating UV laser focused to a 15 μm spot were investigated. With this method, $V_{\rm depletion}$ is identified as the voltage for which the pulse height is $\geq 90\%$ of its maximum.

Table 8: Depletion Voltage of the Detectors Measured by Different Methods

Detector Name	Depletion Voltage Determined by		
	n-side Leakage Current Change (V)	C-V Curve Inflection Point (V)	Maximum Pulse Height (V)
db19	80 ± 4	63 ± 5	55 ± 10
db21	68 ± 2	65 ± 3	60 ± 10
db8	70 ± 2	62 ± 4	55 ± 15
db6	68 ± 4	38 ± 8	60 ± 3
db12	63 ± 4	—*	—†
db29	24 ± 8	16 ± 4	32 ± 10
db27	5 ± 2	6 ± 2	22 ± 15
db30	10 ± 2	17 ± 4	—†

* No inflection point could be found.

† db12 and db30 could not be measured at the laser test stand.

Using the n-side leakage current method has several advantages. It can easily be done by, e.g., the manufacturer, as a quality control step. It is independent of operating read-out electronics; and the inflection point is less ambiguous than that of a C-V curve. To illustrate this latter point, Figure 3 compares the C-V curve and the plot of n-side single strip leakage current versus bias voltage for db8.

The expected (Table 7) and the measured (Table 8, Column 2) values for $V_{\rm depletion}$ agree well for all of the detectors.

2.4 Coupling Capacitance

The effect of the irradiation upon the capacitance of the integrated coupling capacitors was also investigated. The capacitors' dielectric is 100 nm of silicon nitride and 160 nm of silicon dioxide.

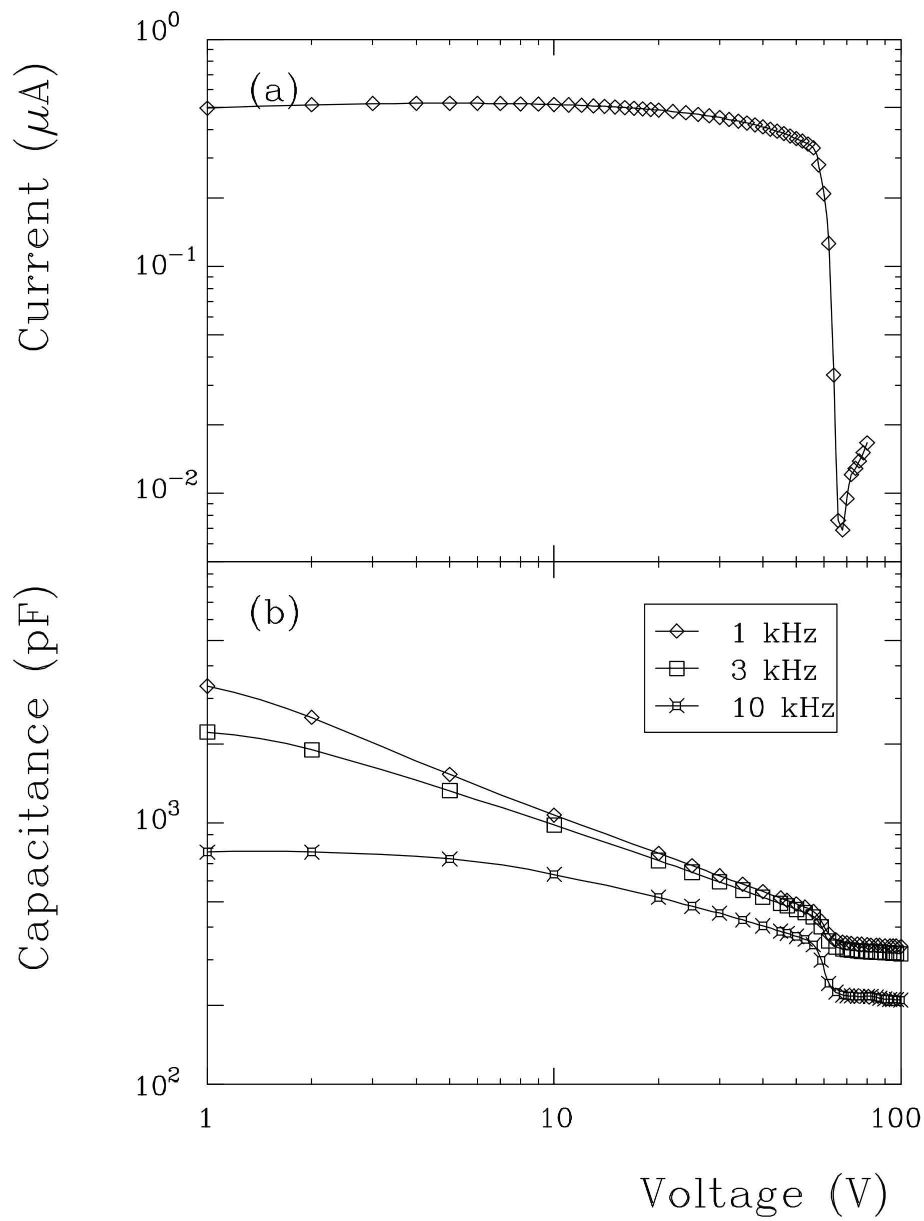

Figure 3: (a) The n-side single strip leakage current and (b) the bulk capacitance, both versus bias voltage for db8.

The experimental setup was based on Figure 8 from Reference [7]. High voltage was applied to the n-side guard ring and bias trace through the n-side connector, and the p-side bias trace was grounded through a probe.

The p-side coupling capacitance was measured on five strips per detector at several frequencies in the range 20 Hz to 1 MHz. The systematic errors on the measurements are the same as those reported in Reference [14]. Measurements were made at 500 Hz. Table 9 indicates that the pre- and post-irradiation values are consistent.

Table 9: p-side Pre- and Post-irradiation Coupling Capacitance Measured with a 500 Hz Signal

Detector Name	Pre-Irradiation Coupling Capacitance (pF)	Post-Irradiation Coupling Capacitance (pF)
db6	162.1 ± 0.8	161.0 ± 0.1
db12	68.6 ± 17.7	86.0 ± 2.1
db29	—‡	74.6 ± 0.6
db27	63.5 ± 7.9	62.5 ± 6.3
db30	79.8 ± 5.2	79.0 ± 0.1

‡ No pre-irradiation data available.

2.5 Total Capacitance

The total capacitance presented to the front-end amplifier was measured directly. One of the constituents of the total capacitance, that due to the bulk, was measured separately when the depletion voltage was studied. A change in the bulk capacitance was observed, so a change in the total capacitance was expected.

The measurements were performed according to the method described in Reference [7]. The positive bias voltage and the high potential terminal of the bias isolation network were both connected to the n-side bias trace and guard ring. The probe attached to the low potential terminal of the bias isolation network contacted an AC pad.

Table 10 shows the total p- and n-side capacitance of the unirradiated and irradiated detectors. The p-side capacitance values are divided by the active length of the implants while the n-side values are not. This difference in treatment reflects the fact that on the p-side, only one layer of metal readout traces contributes to the capacitance, while on the n-side, the second metal is expected to contribute as well. The relative contributions of the two n-side metal layers to the total capacitance depend upon the specifics of their shapes and relative orientations. To aid the reader in applying the n-side results to predictions for other geometries, the fourth column of Table 10 gives the total length of n-side readout strip, both first and second metal, for each sensor. The data in Table 10 have been corrected to compensate for an offset of 1.6 ± 0.3 pF which was found to be associated with mounting the detectors in their boards.

Table 10: Total Capacitance of the Detectors

Detector Name	Total Capacitance		n-side Metal Length (cm)
	per Unit Active Length p-side (pF/cm)	n-side (pF)	
db19	1.0 ± 0.1	7.4 ± 0.4	$2.0^{a} + 4.1^{b}$
db21	1.0 ± 0.1	7.7 ± 0.6	$2.0^{a} + 4.1^{b}$
db8	0.8 ± 0.1	11.6 ± 0.8	$(2^{c} \times 1.3^{a}) + 8.2^{b}$
db6	0.9 ± 0.1	9.1 ± 0.8	$(2^{c} \times 1.3^{a}) + 8.2^{b}$
db12	1.5 ± 0.2	11.4 ± 0.6	$2.0^{a} + 4.1^{b}$
db29	1.4 ± 0.3	11.1 ± 1.3	$2.0^{a} + 4.1^{b}$
db27	1.2 ± 0.1	9.1 ± 0.4	$2.0^{a} + 4.1^{b}$
db30	1.4 ± 0.1	10.2 ± 0.8	$2.0^{a} + 4.1^{b}$

[a] 1st metal; [b] 2nd metal; [c] multiplexing.

Since pre-irradiation data for the individual detectors were not available, detectors within each type[1] were compared with one another. We believe that this is an acceptable comparison to make, since prior to irradiation, detectors of each type were found to exhibit consistent electrical (current and voltage) characteristics. These similarities lead us to assume that the

[1] See Table 1 for the definitions of the types.

pre-irradiation total capacitance values of detectors of the same type do not differ significantly, so that a different total capacitance for an irradiated detector can be attributed to radiation damage.[2]

The total capacitance increased on both the p- and the n-sides with the amount of radiation the detector received. The total capacitance per active length on the p-side increased by $(2.0 \pm 0.7) \times 10^{-14}$ pF-cm/[1 MeV neutron]. The total capacitance on the n-side increased by $(1.5 \pm 0.1) \times 10^{-13}$ pF-cm^2/[1 MeV neutron] for the particular double-metal structure that is described here.

Figure 4 shows the difference in the p-side total capacitance per unit active length between the unirradiated and the irradiated detectors of each type, divided by the received fluence. A straight line is used to show the error-weighted average value.

Figure 5 shows the difference in the n-side total capacitance between the unirradiated and the irradiated detectors, divided by the received fluence. Here detectors of types A and B are used since their n-side designs are identical. Type D detectors are not directly comparable to them on the n-side and so are excluded from the plot. A straight line is used to show the error-weighted average value. Note that this value depends upon the details of the double-metal geometry as well as on the n-side implant dimensions.

3 Conclusions

We have studied some of the electrical properties of silicon microstrip detectors that can be affected by radiation damage. The total leakage currents on the p- and n-sides increase linearly as a function of the fluence of the damaging particles in a manner consistent with the published value of α. For a fluence of damaging particles equivalent to about twice the fluence through a Layer 0 SVX II detector at CDF during the first year of operation, or to the fluence at 12 cm from an interaction point during the first three years of LHC operation, the depletion voltage decreases according to Equation 2. The to-

[2]Reference [7] includes capacitance measurements of a larger sample of unirradiated sensors of this type and confirms the uniformity of capacitance across the batch.

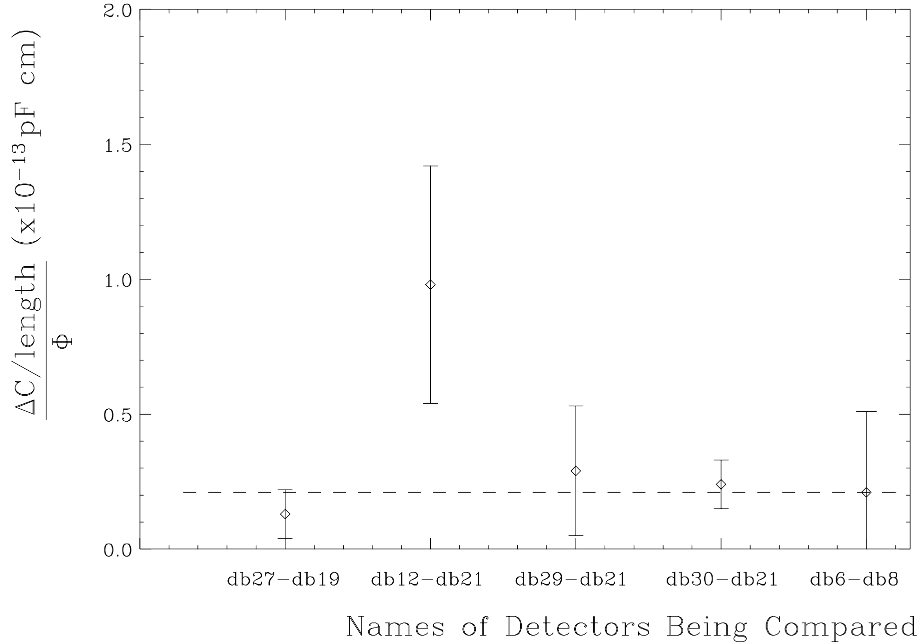

Figure 4: Difference in p-side total capacitance per unit active length between irradiated and unirradiated SVX II prototype silicon microstrip detectors, scaled by the fluence received.

tal capacitance increases on the p-side by $(2.0 \pm 0.7) \times 10^{-14}$ pF-cm/[1 MeV neutron]. The total capacitance on the n-side increases by $(1.5 \pm 0.1) \times 10^{-13}$ pF-cm^2/[1 MeV neutron] for sensors with the double-metal structure that is described here. The coupling capacitance is not affected by this level of radiation.

Acknowledgements

We thank Martin Hoeferkamp for his valuable information about the electronics involved and for his help in optimizing the experimental setup. We thank Tim Thomas for his help in interpreting the results of the measurements. We appreciate the insight that Grant Gorfine and John Matthews have offered concerning phenomena associated with radiation damage. In addition, we thank Nichelle Bruner, Mark Frautschi, Bevin Moon, and

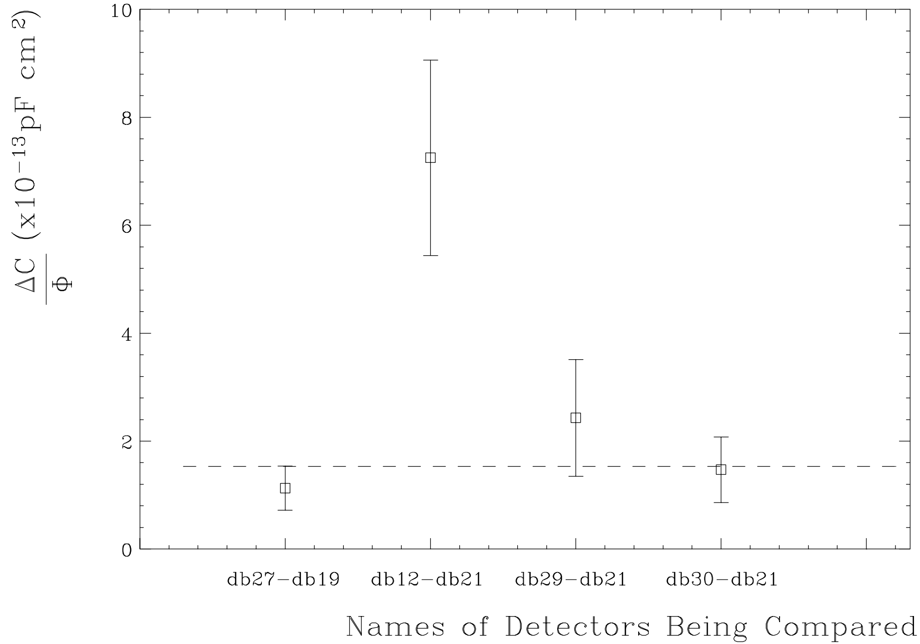

Figure 5: Difference in n-side total capacitance between irradiated and unirradiated SVX II prototype silicon microstrip detectors, scaled by the fluence received.

Aaron Patton for making electrical measurements on some of the detectors.

References

[1] Bacchetta, N., *et al., SVX II Upgrade Proposal & Simulation Study*, CDF Collaboration Internal Note 1922 (1993).

[2] Matthews, J., *et al.*, *Bulk Radiation Damage in Silicon Detectors and Implications for SVX II*, CDF Collaboration Internal Note 3408 (1995).

[3] Gorfine, G. and G. Taylor, *Particle Fluxes and Damage to Silicon in the ATLAS Inner Detector*, ATLAS Internal Note INDET-No-030 (1993).

[4] Seidel, S., *Specifications for SVX II Double-metal Microstrip Detector Prototypes*, CDF Collaboration Internal Note 2030 (1993).

[5] Yarema, R., *et al., A Beginner's Guide to the SVX2*, FERMILAB-TM-1892.

[6] Bruner, N., *et al.*, *Nucl. Instr. and Meth. in Phys. Res.* **A** 362 (1995) 315-337.

[7] Frautschi, M.A., *et al.*, *Nucl. Instr. and Meth.* **A** 378 (1996) 284-296.

[8] Chilingarov, A., *et al.*, *Nucl. Instr. and Meth. in Phys. Res.* **A** 360 (1995) 432-437.

[9] Patton, A., *et al.*, *Electrical Characterization of SINTEF/SI SVX II Prototype Double-sided Silicon Microstrip Detectors*, CDF Collaboration Internal Note 2385 (1994).

[10] Barberis, E., *et al.*, *Nucl. Instr. and Meth. in Phys. Res.* **A** 342 (1993) 373-380.

[11] Feick, H., *et al.*, *Nucl. Instr. and Meth. in Phys. Res.* **A** 377 (1996) 217-223.

[12] Gorfine, G., *et al.*, *Determination of Leakage Currents and Depletion Voltages of Pixel Test Structures*, ATLAS Internal Note INDET-No-139 (1996).

[13] Barberis, E., *et al.*, *Capacitance in Silicon Microstrip Detectors*, Proceedings of the International Symposium on Development and Application of Semiconductor Tracking Detectors, May 22-24, 1993, Hiroshima, Japan, SCIPP 93/16 (1993).

[14] Seidel, S., *et al.*, *Nucl. Instr. and Meth. in Phys. Res.* **A** 383 (1996) 128-136.